Article

Not peer-reviewed version

Solar Geoengineering Potential in Flood Assuagement in Four East African Cities

Herbert O. Misiani , Betty N. Barasa * , Franklin J. Opijah , Hussen S. Endris , Jully O. Ouma , Christopher Lennard

Posted Date: 12 March 2026

doi: 10.20944/preprints202603.0667.v1

Keywords: Eastern Africa; SRM; WACCM; ARISE-SAI; RRI; inundation; flood

 doi:10.20944/preprints202603.0667.v1

Article

Solar Geoengineering Potential in Flood Assuagement in Four East African Cities

Herbert O. Misiani [1], Betty N. Barasa [2]*, Franklin J. Opijah [3], Hussen S. Endris [1], Jully O. Ouma [1], and Christopher Lennard [4]

[1] Climate Diagnostic and Prediction Unit, IGAD Climate Prediction and Applications Centre, Nairobi, Kenya
[2] Logistics and Supply Chain Unit, UN-World Food Programme, Juba, South Sudan
[3] Meteorology Unit, Department of Earth and Climate Sciences, University of Nairobi, Nairobi, Kenya
[4] Department of Envronmental and Geographical Sciences, Univerisity of Cape Town, Cape Town, South Africa
* Correspondence: betiambe85@gmail.com

Abstract

This study evaluates the potential of solar radiation management (SRM) to mitigate projected increases in rainfall and flood risk across four major urban centers in Eastern Africa. Flood dynamics under historical and future climate conditions were simulated using the Rainfall–Runoff–Inundation (RRI) model. Observed hydrological conditions were established using daily precipitation from the Climate Hazards Group Infrared Precipitation with Stations (CHIRPS), together with hydrological and topographic datasets. Future flood projections and associated impacts were derived from climate simulations produced by the Whole Atmosphere Community Climate Model version 6 (WACCM6) and solar climate intervention experiments from the Assessing Responses and Impacts of Solar climate intervention on the Earth system with Stratospheric Aerosol Injection (ARISE-SAI) framework, both forced by the Shared Socioeconomic Pathway SSP2-4.5. Model performance was evaluated using the Nash–Sutcliffe efficiency (NSE), coefficient of determination (R^2), root mean square deviation (RMSD), and peak discharge error (PDE). The RRI model reproduced observed river discharge with reasonable skill, exhibiting lower RMSD and PDE values for the Ethiopian catchment compared to those in Kenya and Tanzania. Results indicate that SRM implemented through stratospheric aerosol injection (SAI) can reduce peak inundation depths and the spatial extent of flooding in selected flood-prone areas of Dar es Salaam and Addis Ababa. These reductions correspond to a decrease in the projected exposure of populations and critical infrastructure to flood hazards. While the findings suggest that albedo-based solar geoengineering may moderate flood impacts in some Eastern African cities, uncertainties remain, particularly in the representation of convective rainfall processes and the reliance on a single hydrological modeling framework in this study. Further research using improved climate simulations and ensemble-based hydrological approaches is recommended.

Keywords: Eastern Africa, SRM, WACCM, ARISE-SAI, RRI, inundation, flood.

1. Introduction

Changes in extreme climate events have been linked to a range of socioeconomic impacts across both global and local scales [1]. While some of these changes can be attributed to the natural variability of the climate system [2], the growing influence of anthropogenic forcing has intensified both the frequency and severity of these events [3,4]. The resulting impacts are being felt worldwide, with particularly severe consequences in already vulnerable communities. Climate model projections suggest that extreme events will continue to increase in both intensity and frequency in the future across different regions [5,6]. Among these, extreme precipitation leading to flooding is of particular concern—estimated to affect between 1.2 and 1.6 billion people globally between 2010 and 2050 by for example increasing their food insecurity [7].

 doi:10.20944/preprints202603.0667.v1

Flooding in Eastern Africa has been associated with substantial socio-economic losses and widespread environmental degradation, including disruptions to ecosystems and biodiversity [8]. The risk is particularly pronounced in major urban centers, where the expansion of impermeable surfaces—especially in densely populated suburban areas—reduces natural infiltration, increasing the likelihood of surface runoff and flash flood risks [9,10]. With urban populations across Africa projected to rise sharply by 2100, and with increasingly intense wet seasons marked by heavy rainfall [11–13], changes in land cover and urban surface characteristics are expected to intensify urban flooding challenges. Flash floods are also prevalent in rural areas—particularly in arid and semi-arid regions—where human-induced landscape changes exacerbate flood risks [14].

For effective adaptation planning, it is essential to understand potential future hydrological extremes, given their significant global impacts [15]. Unlike temperature projections—which consistently show an upward trend—rainfall projections remain highly uncertain across climate models, emission scenarios, and future time horizons, posing a major challenge in quantifying future hydrological extremes [14]. Nonetheless, CMIP6 model outputs project annual rainfall increases of up to 35% in countries such as Ethiopia, Uganda, and Kenya, which could substantially affect streamflow and intensify hydrological extremes across much of Eastern Africa. These changes are expected to have wide-ranging impacts on the region's agriculture, water resources, and energy sectors [16].

Projections indicate that a global temperature increase of 1.5°C above pre-industrial levels could result in economic losses of approximately USD 1.4 trillion annually (equivalent to 0.25% of global GDP) due to sea level rise-induced flooding. At a 2.0°C warming level, these losses are expected to rise sharply, reaching between USD 14 trillion and USD 27 trillion per year by 2100 [17]. Committing to a 2.0°C pathway, rather than limiting warming to 1.5°C, is also projected to increase the frequency of extreme flows in large catchments worldwide [18]. Although there are still large uncertainties associated with these modelling scenarios, the outcomes underscore the urgent need for coordinated global efforts to limit warming to below 1.5°C levels.

Methods for addressing the impacts of climate change are generally categorized into mitigation, adaptation, greenhouse gas (GHG) removal, and solar geoengineering—each with distinct costs, climate impacts, and associated social, economic, and political considerations [19]. Solar geoengineering refers to deliberate interventions in the Earth's radiative balance to counteract some effects of climate change. Techniques under this category include marine cloud brightening (MCB), stratospheric aerosol injection (SAI), cirrus cloud thinning (CCT), surface-based albedo modifications, and space-based approaches [20–25]. Among these approaches, SAI has attracted the greatest attention, partly due to the modelling environment in which it is studied and the significant public debate it has generated regarding its potential climatic, environmental, and socio-political implications [20].

Numerous studies have examined the global and regional climatic responses to SAI and its broader implications for key socio-environmental sectors [26–30]. Evidence from both global and regional scales generally supports the potential of SAI to reduce surface warming; however, its impacts on precipitation remain highly uncertain [28,29]. Several studies suggest a tendency for SAI to suppress land-based rainfall, particularly in monsoon-dominated regions [31]. [30] demonstrated that SAI could reduce flood risk in many regions worldwide, likely due to its suppression of the hydrological cycle—manifested as reductions in mean precipitation—resulting from stratospheric warming via longwave radiation absorption [32,33].

While Solar Radiation Management (SRM) has been proposed as a potentially viable strategy to mitigate some adverse impacts of global warming and extreme climate events [30], its capacity to alleviate or exacerbate projected flood risks in Eastern Africa remains underexplored. This study seeks to address this gap by employing climate model simulations to evaluate the contribution of rainfall extremes to present and future flood hazards in major urban centres across Eastern Africa, under scenarios both with and without SRM deployment.

 doi:10.20944/preprints202603.0667.v1

2. Data and Methods

2.1. Area of Study

This study area covers four urban catchments; each located in a rapidly expanding capital city within East Africa. These sites were selected based on their hydrological importance, flood risk, and socio-environmental complexity. The Nairobi River Catchment in Nairobi, Kenya, originates from the Ondiri Swamp in Kikuyu and flows eastward through the city, eventually joining the Athi River. It consists of several tributaries, including the Ngong, Mathari, and Gitathuru Rivers, with narrow channels and canalized sections traversing the central business district [34,35]. The Msimbazi River Catchment in Dar es Salaam, Tanzania, begins in the Pugu Hills and passes through the Ilala and Kisarawe local government areas before discharging into the Indian Ocean near Selander Bridge. This area features a densely populated floodplain with essential transport infrastructure and was historically protected by a wetland buffer zone. The Nakivubo Channel Catchment in Kampala, Uganda, serves as the main drainage system through the city's commercial core and was originally engineered for flood mitigation. It operates as an open trench receiving stormwater, sewage, and industrial effluent. Lastly, the Big Akaki River Catchment in Addis Ababa, Ethiopia, rises in the Ethiopian Highlands, flows through Addis Ababa, and merges with the Awash River. It includes both the Little and Great Akaki tributaries, covers an area of approximately 1,682 km^2, and is crucial for urban water supply and the biodiversity of the Akaki–Aba-Samuel wetlands.

All the four East Africa cities have experienced periodic flooding, largely attributed to geographic location as well as rapid urbanization, Figure 1. The cities are situated in regions which are susceptible to very heavy seasonal rainfall, often leading to rivers overflowing.

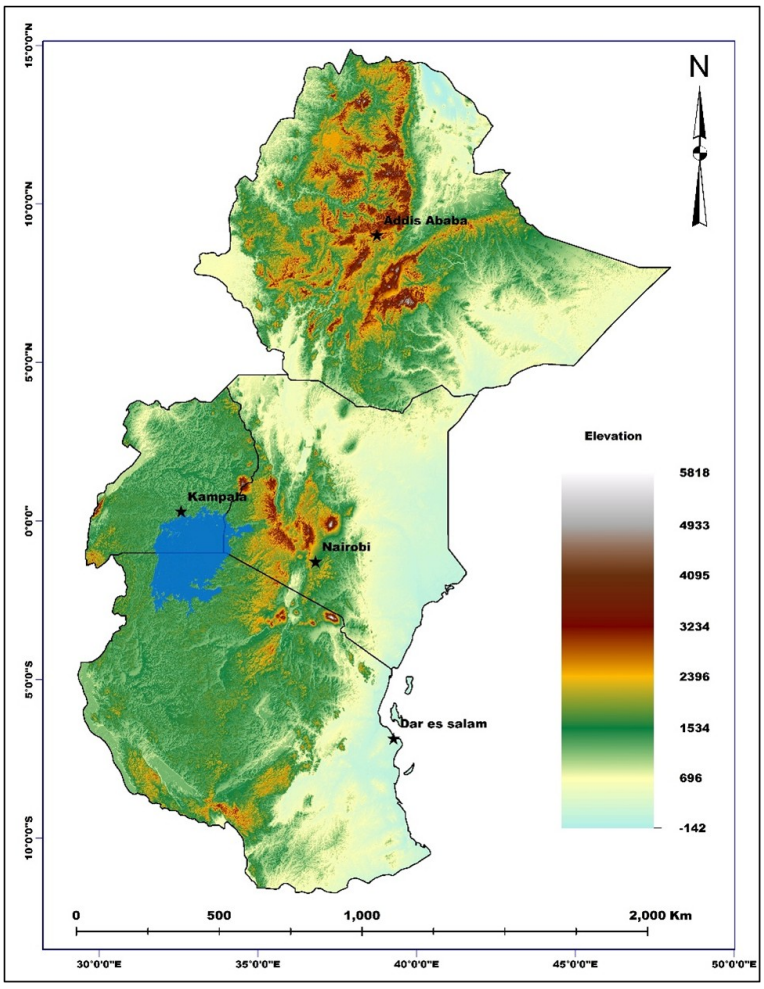

Figure 1. Topography and the location of cities of Addis Ababa (A), Kampala (K), Nairobi (N), and Dar es Salaam (D).

 doi:10.20944/preprints202603.0667.v1

2.2. Rainfall, Discharge and Water Level Reference Data

To accurately simulate flooding scenarios in the selected East African cities, this study adopted a multi-faceted approach integrating climate, hydrological, and topographical datasets. The quasi-global Climate Hazards Group Infrared Precipitation with Stations (CHIRPS) dataset was employed both to evaluate climate model performance and to initialize the hydrological model at five representative points within each of the four cities. CHIRPS provides a high-resolution (0.05°) daily gridded rainfall time series that blends in-situ station observations with satellite-derived estimates, spanning 1981 to the near-present and covering latitudes from 50°S to 50°N. This dataset is widely used for analysing rainfall variability, detecting long-term trends, and monitoring seasonal droughts [36]. River discharge and water level data were sourced from the Ministry of Water of Ethiopia, the Water Resources Authority of Kenya, and the Ministry of Water of the United Republic of Tanzania.

2.3. Elevation, Land Cover, and River Channel Geometry

Flow direction, flow accumulation, and digital elevation model (DEM) datasets were acquired from the United States Geological Survey (USGS) Earth Explorer platform (https://earthexplorer.usgs.gov/) at a spatial resolution of 1 arc-second (30 m). Land cover classification was derived from the Global Land Cover Characterization (GLCC-V2) dataset, reclassified into three aggregated categories—cropland and pasture, forest and woodland/grassland mosaic, and water bodies—out of the nine original GLCC-V2 classes. This reclassification provided the basis for parameterising surface and subsurface hydrological processes in accordance with the Green–Ampt infiltration approach (Richards, 1931). For the hydraulic geometry, a rectangular channel cross-section was assumed, with embankment height set to zero, river widths and depths were estimated from Google Earth Pro imagery. Figure 2 presents the DEM for the study areas, which was used to delineate catchment boundaries and used to derive hydrodynamic modelling parameters such as flow direction and accumulation.

 doi:10.20944/preprints202603.0667.v1

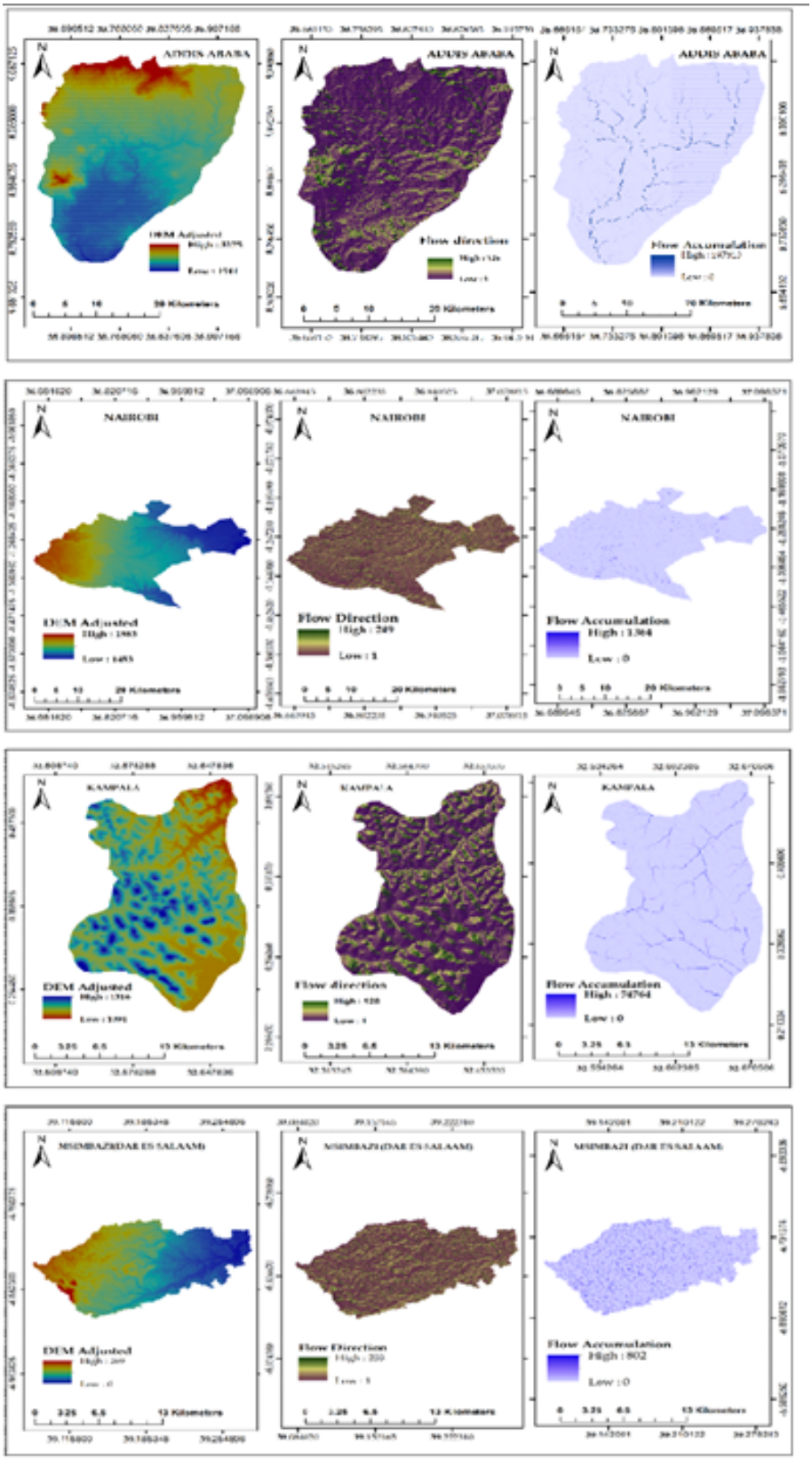

Figure 2. Digital elevation data for the major cities in the study area: Addis Ababa (first row), Nairobi (second row), Kampala (third row), and Dar es Salaam (fourth row). The left, middle and right panels show, respectively, the adjusted digital elevation model data, the flow direction, and the flow accumulation.

 doi:10.20944/preprints202603.0667.v1

2.4. Downscaling of Climate Projections

The climate projection dataset was statistically downscaled using a quantile mapping (QM) technique to improve its spatial fidelity and ensure its suitability for local-scale hydrological modelling. The method adopted was a distribution-based, direct, and parameter-free quantile mapping approach following the formulation of [37]. Quantile mapping was implemented at a daily time step (t) for each grid cell (i), yielding a bias-corrected time series $Y^c or$ according to Equation 1. The correction was applied individually to each grid point using a correction function (CF) derived from the deviation between the observed and modelled inverse empirical cumulative distribution functions $(ecdf)$ for the corresponding day of year (doy) within the calibration period (cal), at a given probability P (Equation 2).

$$Y_{t,i}^{\text{cor}} = X_{t,i}^{\text{raw}} + CF_{t,i} \tag{1}$$

$$CF_{t,i} = \text{ecdf}_{\text{doy},i}^{\text{obs,cal}^{-1}} - \text{ecdf}_{\text{doy},i}^{\text{mod,cal}^{-1}}(P_{t,i}) \tag{2}$$

$$P_{t,i} = \text{ecdf}_{\text{doy},i}^{\text{mod,cal}}(X_{t,i}^{\text{raw}}) \tag{3}$$

The probability P is derived by mapping the raw climate model output (X^{raw}) to its corresponding inverse empirical cumulative distribution function (ecdf) computed over the calibration period (Equation 3). The day-of-year (doy) is centred within a 31-day moving window, which is employed to construct a distinct ecdf for each doy to account for intra-annual variability. All statistical downscaling and bias correction procedures were implemented using the Xclim climate data processing library in Python v3.1 [38]. The two datasets were each subset into two: 1981-2010 and 2011-2015 (the fit and test periods respectively). The downscaling methodology was based on the empirical quantile mapping (EQM), through the Xclim Python package, applied to each month and grid ([39]) (Logan, et al., 2022). This was only possible after interpolating the model data onto the observed (CHIRPS) grid using bilinear interpolation method. The bias-corrected data was used in the analysis of flash flood scenarios in the three East African Cities.

2.5. Rainfall-Runoff Inundation Modelling

The two-dimensional Rainfall–Runoff–Inundation (RRI) model provides a physically based framework for simulating hydrological and flood processes by resolving surface flow, vertical infiltration, lateral subsurface flow, and riverine flooding within a gridded domain [40,41]. The model distinguishes between slope and channel processes, discretising river channels along the centreline of each grid cell while accounting for the overlying slope. Flow dynamics in the slope and channel components are represented using discretised two- and one-dimensional diffusive wave formulations, respectively, based on the conservation of mass and momentum for gradually varied unsteady flows [42,43].

The Rainfall Runoff Inundation (RRI) model, a two-dimensional hydrological model, is specifically designed to simulate both rainfall and runoff processes simultaneously across complex terrains. By incorporating the interactions between precipitation, surface flow, and river discharge, the RRI model provides detailed spatial and temporal patterns of inundation, making it an asset for flood risk assessment in urban and peri-urban settings.

The RRI model has been widely applied across diverse hydrological settings. For example, [44] demonstrated its utility in simulating flood inundation in the Upper Citarum River watershed in West Java, Indonesia, where inundation extent was reproduced satisfactorily however, they showed that simulated discharge exhibited discrepancies attributable to uncertainties in observed records and limitations in initial condition data. Similar strengths have been reported in other regions, including Pakistan [41], Sri Lanka [45], and Thailand [46], where the model consistently reproduced inundation extent with reasonable accuracy. Nonetheless, several studies have emphasized its limitations, particu-

 doi:10.20944/preprints202603.0667.v1

larly in reproducing inundation depth and discharge, due in part to the omission of evapotranspiration processes [46].

As the RRI model is inherently event-based, its application is constrained to relatively short simulation periods, typically not exceeding 90 days. To address this limitation, key flood-contributing events were identified within both the historical and projection datasets to optimize computational efficiency and focus resources on the most critical periods. Specifically, the maximum daily precipitation during the principal rainfall seasons of each study city was used as a trigger event: March–May for Kenya and Uganda, July–September for Ethiopia, and March–May for Tanzania. Thirty-day windows centred on these maximum precipitation events were subsequently extracted from a climatological period (30 years) and used for model simulations in both historical and future scenarios.

To reduce the dimensionality of the simulation outputs, the ensemble mean, and standard deviation of inundation extent were computed for both the stratospheric aerosol intervention (SAI) and non-SAI experiments. Spatial variability within the ensemble was quantified through the standard deviation of inundation depth across ensemble members for each experimental configuration.

Model performance was evaluated by assessing the ability of the RRI model to replicate observed river discharge. Several statistical metrics were employed to ensure a comprehensive evaluation: the Nash–Sutcliffe Efficiency (NSE), which measures the proportion of residual variance relative to the observed variance; the coefficient of determination (R^2) as a measure of collinearity [47]; the index of agreement, which accounts for proportional differences between observed and simulated values [48]; and the root mean square deviation (RMSD), which captures the average magnitude of prediction errors. In addition, the peak discharge error (PDE) was calculated as the percentage difference between observed peak discharge (Q_o) and simulated peak discharge (Q_s) (Equation 4).

$$\mathrm{PDE} = \frac{Q_s - Q_o}{Q_o} \times 100 \tag{4}$$

Flood inundation risk assessment was conducted to identify areas with elevated vulnerability to flooding, thereby supporting the prioritization of mitigation strategies and reducing adverse socio-economic consequences. The assessment was designed to provide evidence-based insights to inform decision-making processes related to emergency response planning and infrastructure development. The analysis employed zonal statistics to quantify the impacts of inundation on exposed populations and critical infrastructure.

3. Results

We discuss the results with respect to the inter-annual variability of rainfall, effectiveness of the RRI model to simulate and identify flooding hotspots, rainfall downscaling and bias correction, extent of historical and future flooding, and simulated inundation depths and flood risk assessment in the major cities of Eastern Africa.

3.1. Inter-Annual Rainfall Variability Over the Cities of Eastern Africa

The inter-annual variability of rainfall across four representative stations in each of the four major cities in Eastern Africa, expressed as departures from the long-term mean (LTM) for the period 1981–2010, is illustrated in Figure 3 for the years 1981–2020. At Entoto station in Addis Ababa, Ethiopia, the rainfall distribution reveals pronounced anomalies (Figure 3a). The years 1997, 2014, and 2015 were among the driest, recording deficits of more than 200 mm below the LTM, while 1990, 1996, 1998, 2010, 2019, and 2020 were the wettest, with surpluses exceeding 200 mm above the LTM. Notably, 2015 and 2020 represent the driest and wettest years, respectively, during the study period.

These extremes can partly be linked to large-scale climate drivers. In particular, the El Niño–Southern Oscillation (ENSO) appears to play a critical role. Previous studies have demonstrated that Ethiopian rainfall is significantly influenced by ENSO, with suppressed rainfall frequently associated with El Niño events and enhanced rainfall during La Niña phases, especially in the primary rainfall season of June–September [49].

 doi:10.20944/preprints202603.0667.v1

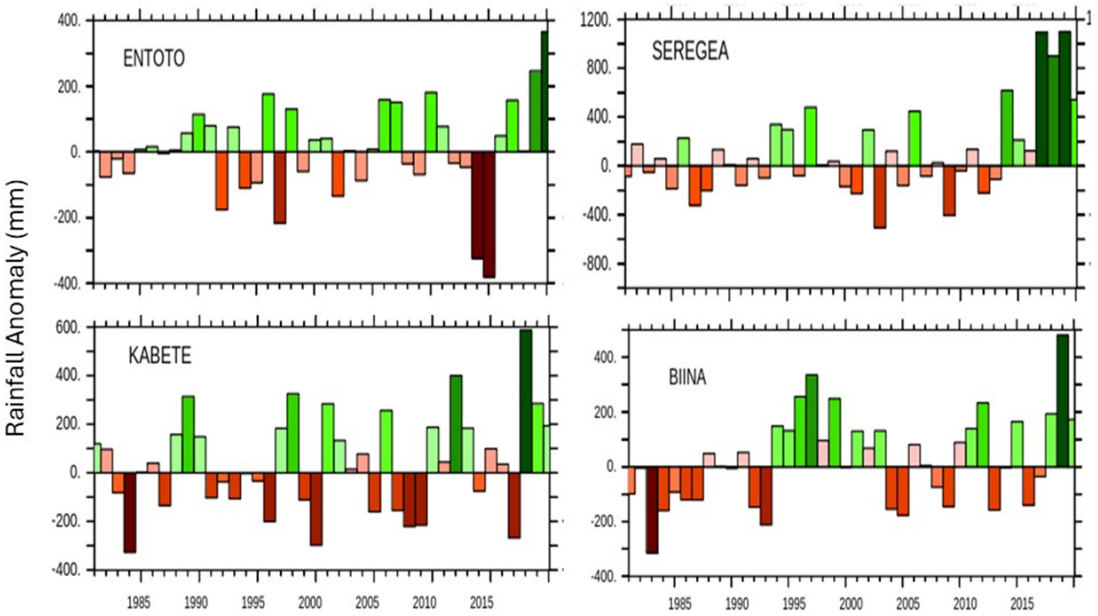

Figure 3. Annual rainfall anomalies for five stations over Dar es Salaam, Tanzania over the period 1981-2017 based on the long-term mean for 1981-2010. Rainfall deficits (surplus) are represented by brown (green) bars respectively. The years 2003 (2017, 2018, and 2019) recorded the least (highest) rainfall over the period for all the stations.

In Seregea Tanzania, the highest (lowest) rainfall occurred in 2015, 2017, 2018, and 2019 (1987, 2004, 2009); 2017 and 2019 were wettest years with more than 800 mm above the LTM (Figure 3b). The departure from the mean for the driest years was not as pronounced as for the wettest years. For Kabete Kenya (Figure 3c), the least (highest) rainfall was recorded in the years 1984, 1996, 2000, 2008, 2009 and 2017 (2012, 2018, 2019 and 2020). The highest rainfall in 2018 was associated with the MAM (long-rains wet season), one of the wettest years on record that resulted in flooding, including in the city [50]. Figure 3d, shows the variability of rainfall over Biina station in Kampala Uganda suggesting a periodicity in the epochs of rainfall deficits and enhancements. The lowest rainfall amounts were observed in the early 1980s and between 2004 and 2016, while the highest rainfall amounts were observed between 1995 and 2003, and the recent three years from 2018-2020. The lowest rainfall amount was recorded in 1983, and the highest in 2019.

3.2. Effectiveness of the RRI Model to Simulate and Identify Flooding Events

Figure 4 to Figure 9 show the simulated and river gauged discharge hydrographs and best fit scatter diagrams for the major rivers in the largest cities in Eastern Africa as simulated by the RRI model. The simulation was done based on daily CHIRPS data, extracted for the stations, as the reference data.

 doi:10.20944/preprints202603.0667.v1

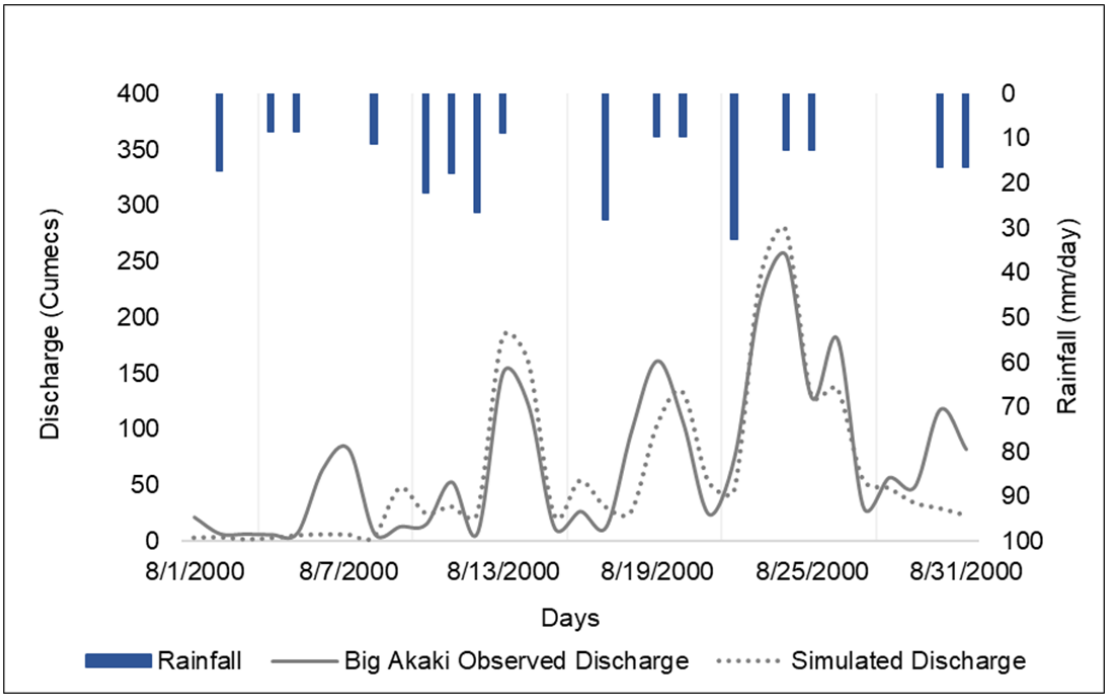

Figure 4. Gauged river discharge hydrograph (solid grey line), simulated discharge from the RRI (dashed grey line) and the corresponding observed rainfall. The figure shows a lag in catchment response to observed rainfall for the Big Akaki River in Addis Ababa.

The results indicated inundation near the confluence of the Big and Small Akaki Rivers in Addis Ababa. The simulated and observed hydrograph for the Big Akaki River agreed well, although there was a tendency for the model to overestimate the peaks compared to the observed discharge (Figure 5).

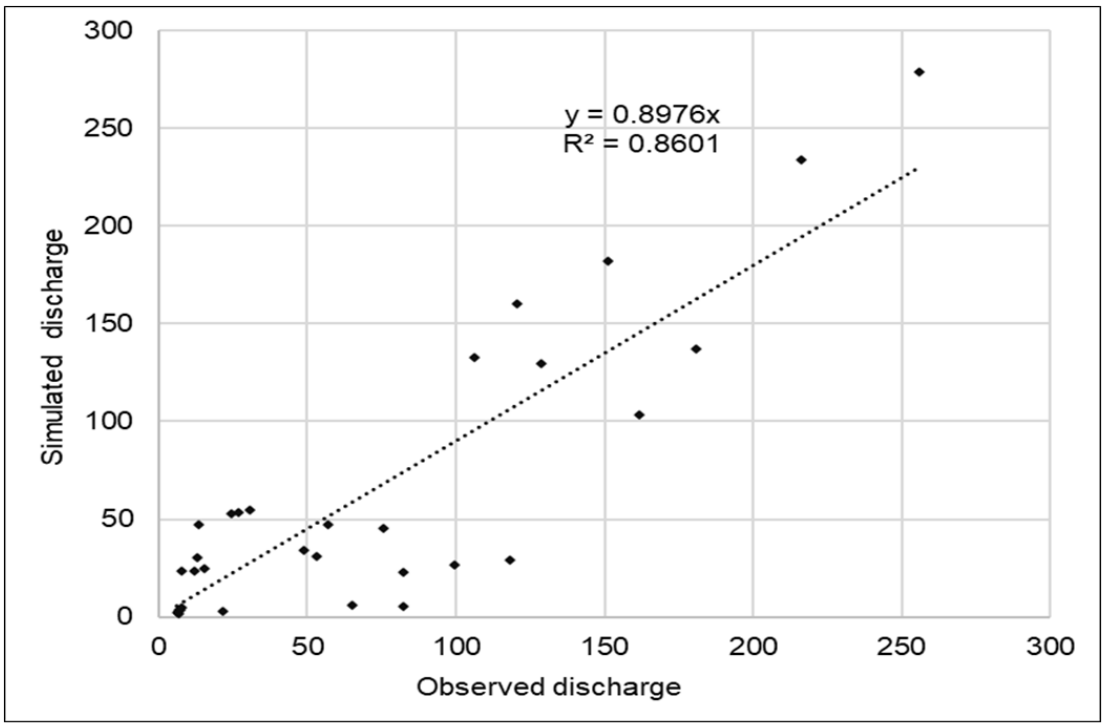

Figure 5. The best line fit scatter diagram for the Big Akaki River in Addis Ababa showing a good correlation between the simulated and the observed discharges.

 doi:10.20944/preprints202603.0667.v1

In Dar es Salaam Tanzania, the simulated and observed hydrographs agreed for the Msimbazi River at Kigogo Bridge, especially, during the April 2020 event, as illustrated in Figure 6. The high peak flow during this time was approximately 288.78 m^3/s equivalent to a 2.5-meter water level. Figure 7 shows the best fit scatter diagram for the simulated and observed hydrograph for the Msimbazi River.

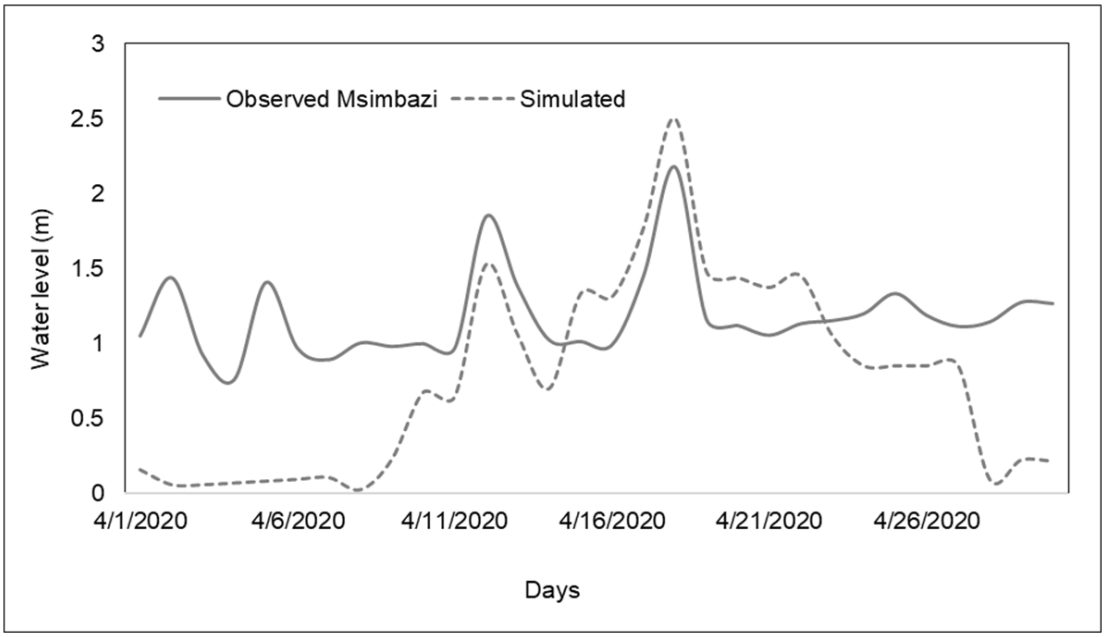

Figure 6. Gauged river discharge hydrograph (solid grey line), simulated discharge from the RRI (dashed grey line) and the corresponding observed rainfall. The figure shows a lag in catchment response to observed rainfall for the Msimbazi River (Kigogo Bridge) in Dar es Salaam.

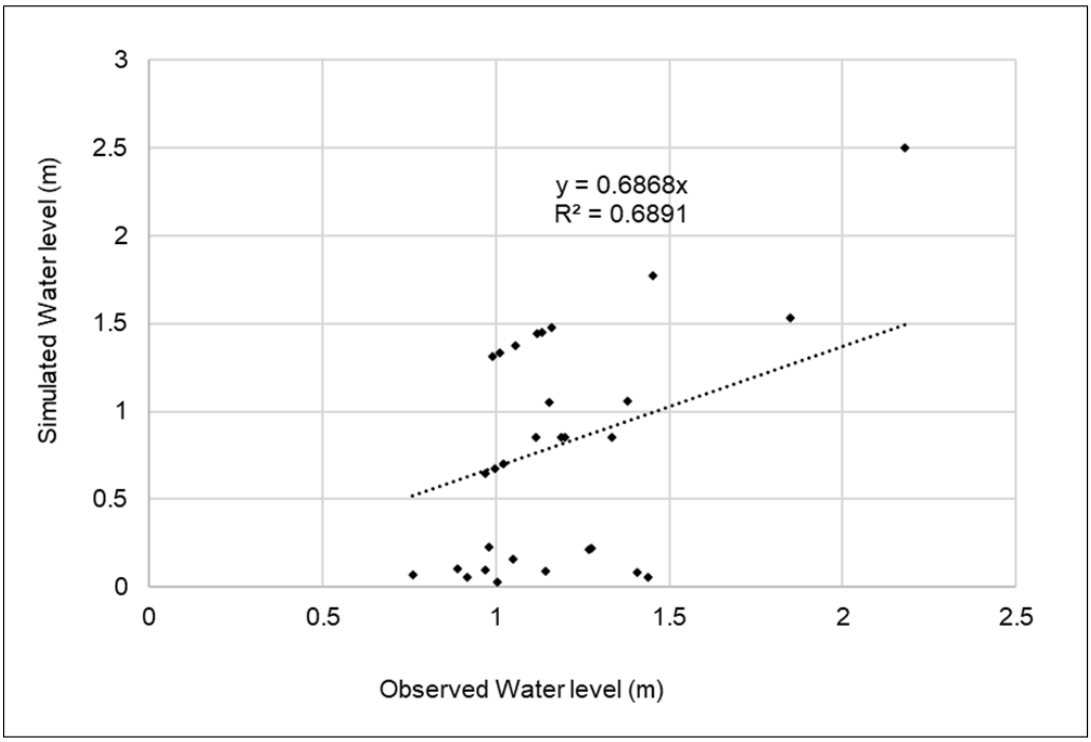

Figure 7. The best line fit scatter diagram for the Msimbazi River (Kigogo Bridge) in Dar es Salaam showing poor correlation between the simulated and the observed discharges.

 doi:10.20944/preprints202603.0667.v1

Figure 8 shows the simulated and observed discharge for Nairobi River and the corresponding correlation coefficients. The simulated peak discharge matched the observed flood within Nairobi City. During extreme rainfall events, higher river flows frequently exceed the banks of the Nairobi River, leading to widespread inundation of adjacent areas. Local dailies have in the past reported significant impacts in the peri-urban neighbourhoods, where floodwaters disrupted livelihoods, damaged infrastructure, and heightened concerns about public health and safety. These flooding episodes underscore the vulnerability of urban and peri-urban communities along the Nairobi River, highlighting the urgent need for effective flood risk management strategies and early warning systems [51]. Figure 9 shows the best fit scatter diagram for the simulated and observed hydrograph for the Nairobi River.

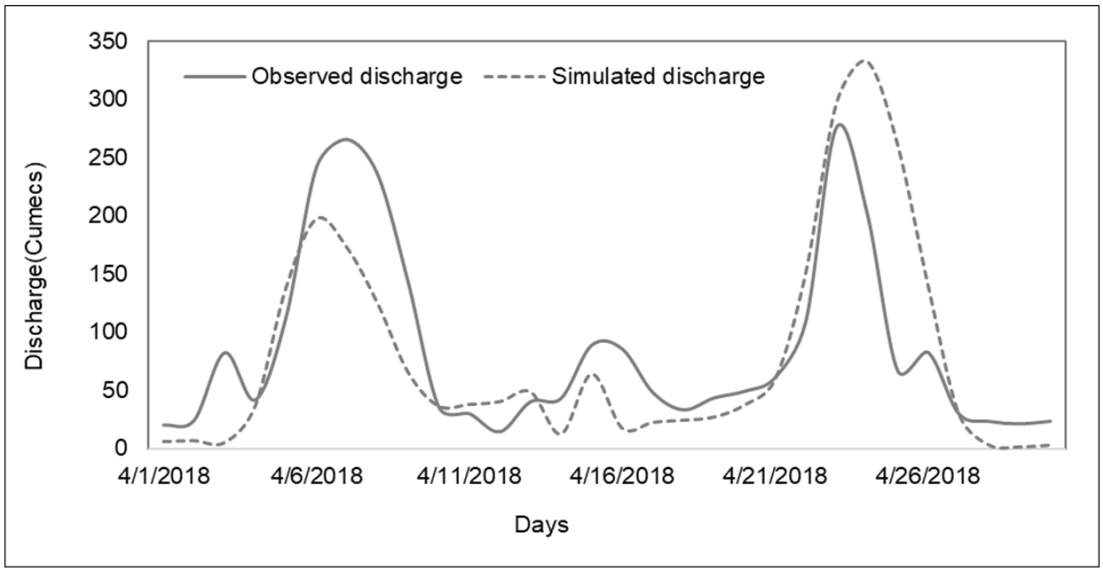

Figure 8. Gauged river discharge hydrograph (solid grey line), simulated discharge from the RRI (dashed grey line) and the corresponding observed rainfall. The figure shows a lag in catchment response to observed rainfall for the Nairobi River in Kenya.

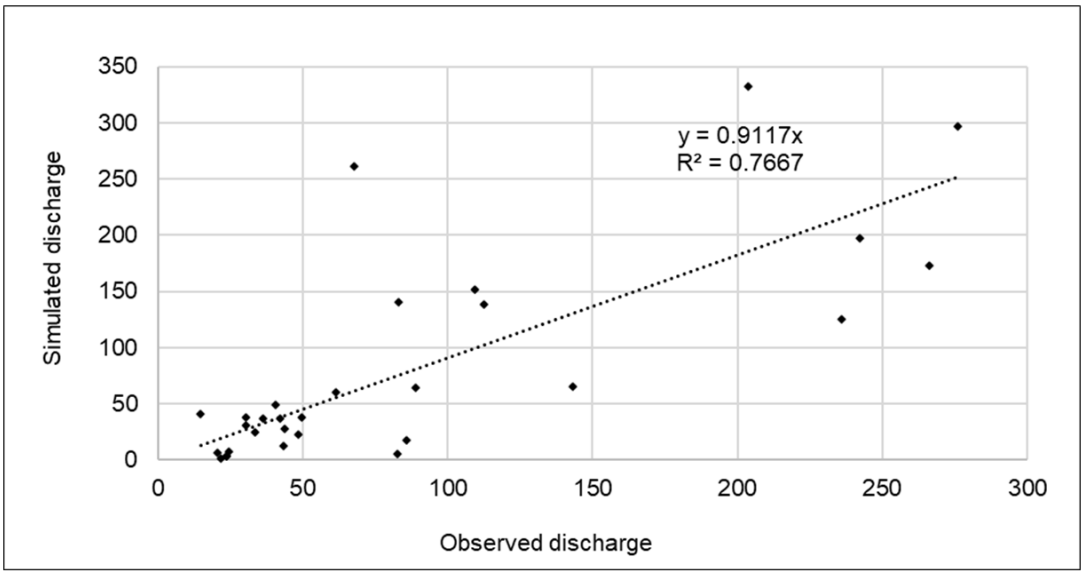

Figure 9. The best line fit scatter diagram for the Nairobi River in Kenya showing poor correlation between the simulated and the observed discharges.

 doi:10.20944/preprints202603.0667.v1

The skill of the RRI model in simulating discharge is summarized in Table 1 using four metrics: Nash-Sutcliffe Efficiency (E), Coefficient of determination (R2), Root Mean Square Deviation (RMSD) and Peak discharge error (PDE). The table shows high correlation coefficient indicating strong linear association between the model and the observed discharge. The error in the simulated peak discharge was lowest for Akaki River (8.96%) and highest for Nairobi River (20.5%) as shown by the PDE scores.

Table 1. Model performance metrics for the River Catchments in three Major Cities of the Eastern Africa.

Efficiency Parameter	Big Akaki	Msimbazi	Nairobi River
Nash-Sutcliffe Efficiency (E)	0.699	0.505	0.419
Coefficient of determination (R^2)	0.753	0.689	0.767
Root mean square deviation (RMSD)	0.360	0.665	0.590
Peak discharge error (PDE) (%)	8.96	14.00	20.50

3.3. Rainfall Downscaling and Bias Correction

Figure 10 presents the spatial distribution of observed rainfall from CHIRPS, together with the biases of the raw model output and the bias-corrected (downscaled) rainfall for April, May and June. The observed rainfall patterns indicate a seasonal progression: during April, rainfall is concentrated over the equatorial belt and parts of the southern sector; in May, the maxima shift toward the western and coastal equatorial regions and central Ethiopia; while in June, rainfall is predominantly confined to the northern sector, particularly South Sudan and Ethiopia (Figure 10a, d, g).

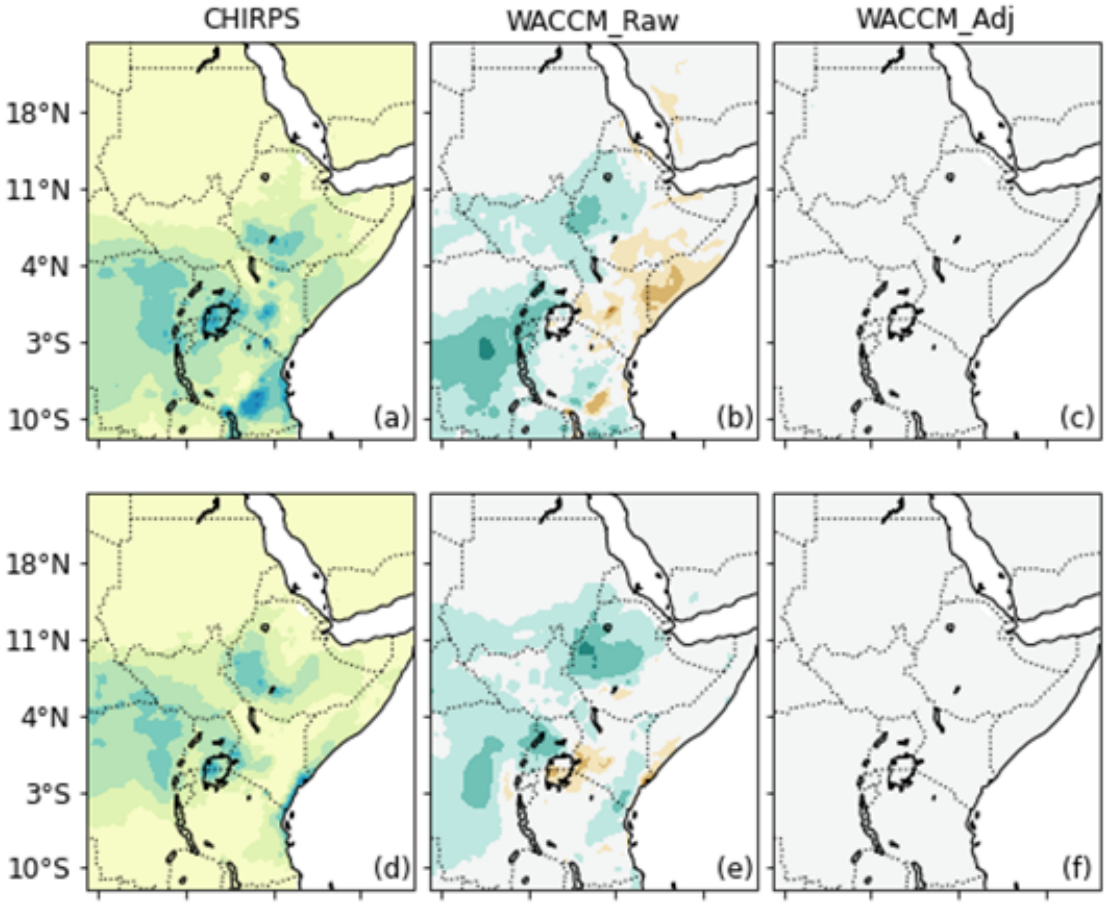

Figure 10. *Cont.*

 doi:10.20944/preprints202603.0667.v1

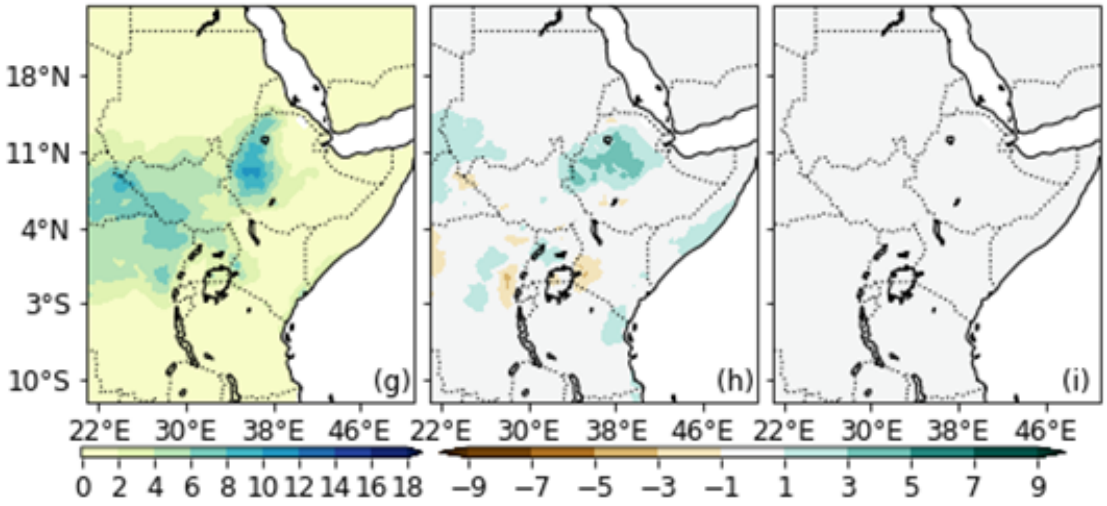

Figure 10. Downscaled and bias corrected rainfall plots over the study area for April (first row), May (second row), and June (third row). The first column shows the observed data; the second and the third columns show the results of the raw and adjusted model biases, respectively.

The raw model simulations exhibit substantial biases across the region. In April, the model generally overestimates rainfall in the northern, western, and isolated southern areas, while markedly underestimating over much of Kenya, southeastern Ethiopia, and southern Somalia. In May, underestimations are evident across the Ethiopian highlands, western Uganda, and southeastern Kenya, whereas slight overestimations occur in parts of the eastern Lake Victoria Basin. By June, the raw model continues to overestimate rainfall across the Ethiopian highlands (Figure 10b, e, h).

Application of the quantile mapping (QM) procedure substantially reduces these biases across all months (Figure 10c, f, i). Nevertheless, the model consistently demonstrates a tendency to overestimate rainfall over high-elevation areas, particularly the Ethiopian highlands. This systematic bias is likely attributable to challenges in how the model represents orographic rainfall processes.

3.4. Impact of SAI on Simulated Peak Discharge and Inundation Depth

A comparative analysis of the peak discharge and inundation depth using historical, simulations without albedo modification and those with albedo modification was carried out as shown in Figure 11 to Figure 14.

In Ethiopia, the simulations in the historical period were based on the six different peak discharges from diverse epochs. The 1997-1998 El Niño which affected most of East Africa was considered the worst-case scenario with the highest peak discharge on the basin under consideration. It is, however, important to note that observed inundation depths for this period were not available for comparison. The results indicated that inundation depths and peak discharge reduced under the SAI scenario compared to the simulations without albedo modifications. The discharge decreased from 233.30 m^3/s under the global warming scenario to 194.38 m^3/s under SAI, Figure 11.

 doi:10.20944/preprints202603.0667.v1

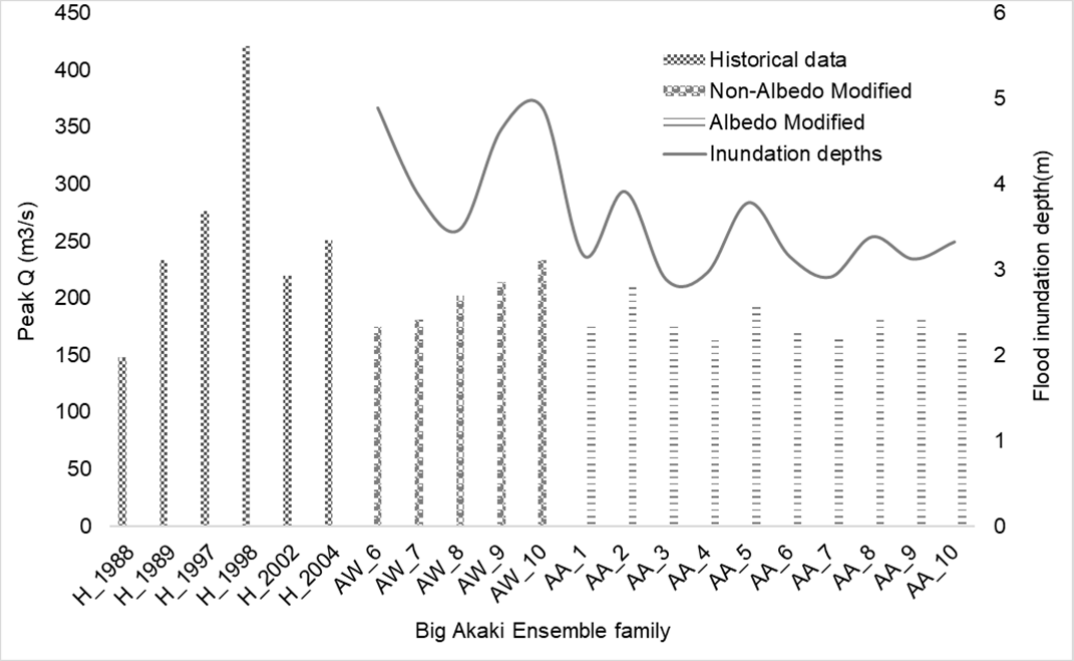

Figure 11. Peak discharges for observed, WACCM6 and ARISE-SAI 4.5 (bar graphs) versus peak inundations (solid grey line) for Akaki River Basin, Addis Ababa City.

Inundation peaks for Addis Ababa City on the other hand reduced by 20.04% using the modified albedo ARISE-SAI 4.5 data. The peak inundation depth dropped from 4.89m to 3.91m. Albedo modification played a fundamental role in reducing the peak discharges and inundation depths on the basin. Downscaled rainfall gave diverse years for flood occurrences on the basin. The ARISE-SAI 4.5 and the WACCM dataset varied in the years that exhibited extreme rainfall events in Ethiopia, Figure 11.

Simulation results obtained for the Nairobi City in Kenya (Figure 12) indicated a consistency in inundation depths with declining peak discharges using ARISE-SAI 4.5 rainfall (with albedo modification) as compared with the WACCM 4.5 rainfall (without modification of albedo). There was no significant change in the inundation peaks on the basin using the different downscaled datasets; the percentage difference in the highest simulated peak inundations using ARISE-SAI 4.5 and WACCM was 6.98%. However, the simulated peak discharges using the ARISE-SAI 4.5 albedo modified dataset as compared to the WACCM dataset with a percentage decline of 47.44% which was almost half of the discharge using albedo modification. The discharge decreased from 171.218 to 89.99 using modified ARISE-SAI 4.5 dataset. It was also noted that the observed peak discharges on the basin, especially the El Niño related rains, was more than four times both the observed and simulated results for both ARISE-SAI 4.5 and WACCM 4.5 datasets, but this value was omitted in the final analysis. Albedo modification played a fundamental role in reducing the peak discharges. However, the inundation depths on the basin were consistent using the 2 datasets under consideration.

 doi:10.20944/preprints202603.0667.v1

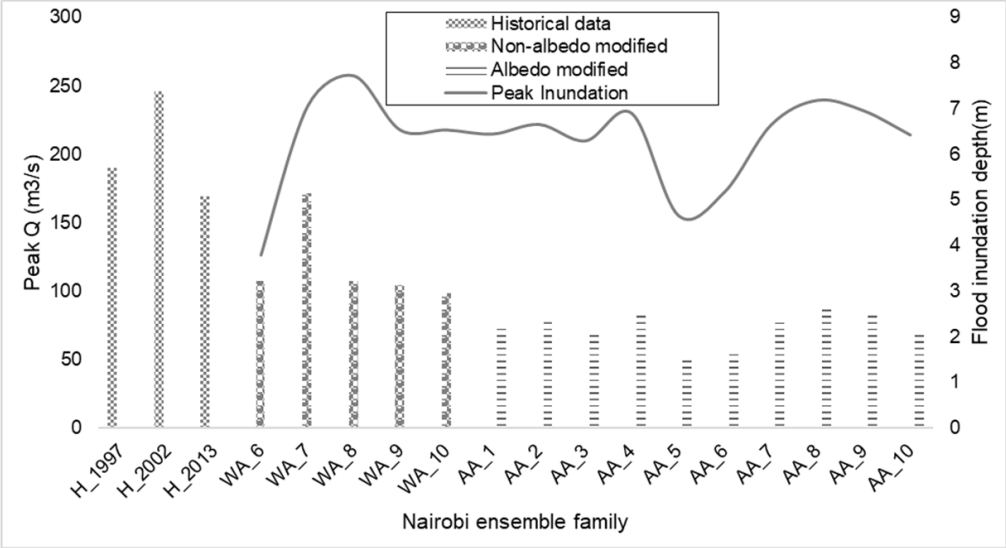

Figure 12. Peak discharges for observed, WACCM and ARISE-SAI 4.5 versus peak inundations (solid grey line) for Nairobi River Basin, Kenya.

In comparison to the WACCM rainfall without albedo modification, the simulation results obtained for Msimbazi River in Dar es salaam, Tanzania (Figure 13), showed a decline in inundation depths with falling peak discharges while utilizing the ARISE-SAI 4.5 rainfall (with albedo modification). The maximum simulated peak inundations using ARISE-SAI 4.5 and WACCM differed by 57.68%; there was visible change in the inundation peaks and discharges using the ARISE-SAI 4.5 albedo modified downscaled datasets. It was also noted that using the downscaled dataset for CMIP6-SSP2-4.5-WACCM 8 for Dar es salaam this ensemble family had extremely above normal rainfall of over 500mm rainfall in a single event which gave a very high peak discharge with inundation depth of over 9 meters. The discharge utilizing the downscaled ARISE-SAI 4.5 dataset dropped from 693.77 m^3/s to 293.58 m^3/s which accounted for 57.68% decline in the peak discharge received on the basin (Figure 13).

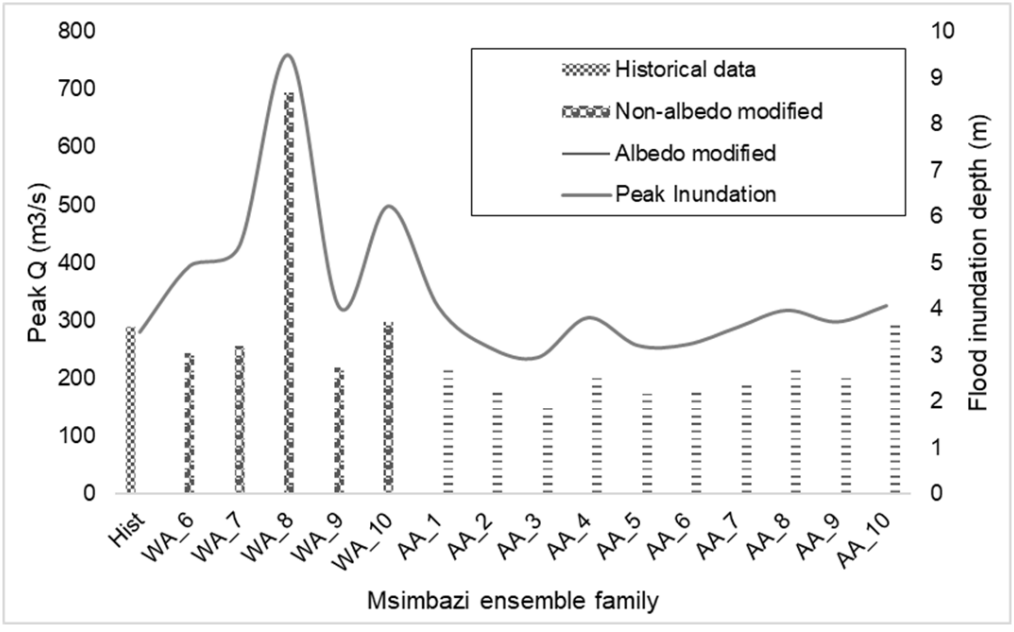

Figure 13. Peak discharges for observed, WACCM and ARISE-SAI 4.5 versus peak inundations (solid grey line) for Msimbazi River Basin, Dar es Salaam City Tanzania.

 doi:10.20944/preprints202603.0667.v1

Simulation for Nakivubo channel in Uganda was undertaken even though the observed data was not available for effective model calibration and validation. However, modelled numerical results indicate no change in the behavior of discharge and inundation depths (Figure 14).

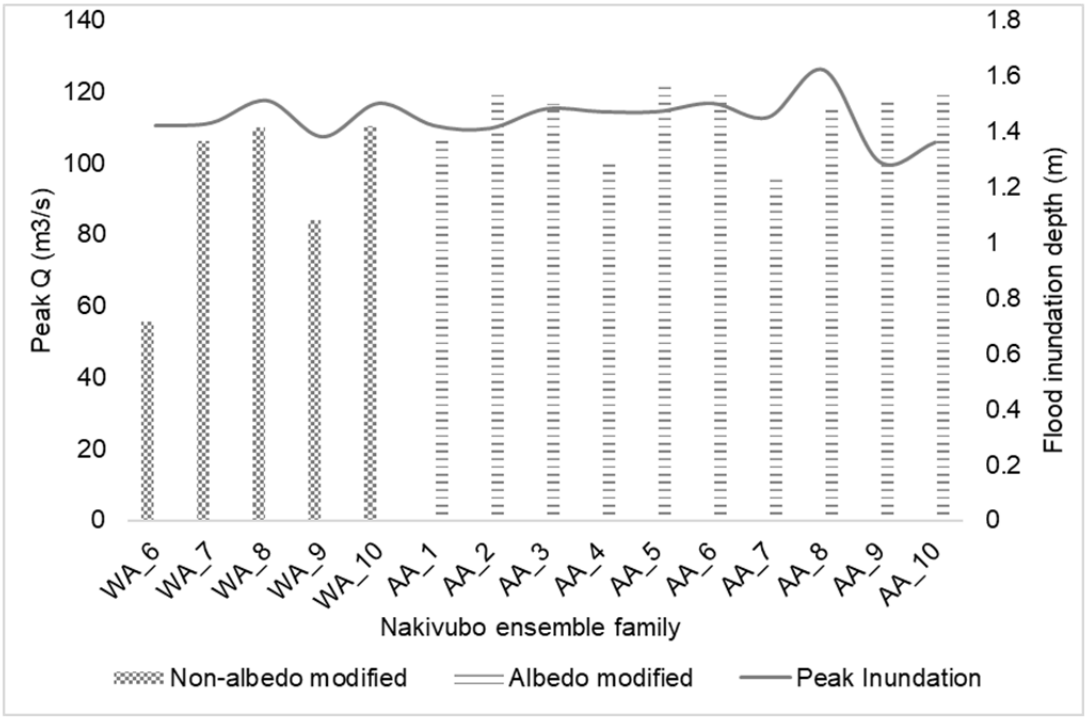

Figure 14. Peak discharges for observed, WACCM and ARISE-SAI 4.5 versus peak inundations (solid grey line) for Nakivubo River Basin, Kampala City Uganda.

3.5. Simulated Extent of Flood Inundation Depths and Flood Risk Assessment over Major Cities of Eastern Africa

This section presents the simulated spatial distribution of flood inundation depths under both albedo-modified and non-albedo conditions, together with estimates of the population and infrastructure exposed to flood hazards under the non-albedo scenario across the four major cities of Eastern Africa. For Addis Ababa, flood projections indicate substantial spatial variability in inundation depth, with simulations under the global warming scenario without albedo modification exhibiting the most extensive flooding, including areas experiencing inundation depths exceeding 2m (Figure 15a). By contrast, simulations incorporating albedo modification show a marked reduction in the spatial extent and severity of inundation (Figure 15b). These results highlight the potential effectiveness of albedo-based interventions in reducing flood exposure and mitigating urban flood risk under future climate conditions.

Similar patterns are observed in Dar es Salaam, where projections under the global warming scenario without albedo modification indicate extensive flooding, with water depths surpassing 2 meters (Figure 16a). By comparison, albedo-modified simulations show a reduction in the areal extent of inundation water (Figure 16b).

 doi:10.20944/preprints202603.0667.v1

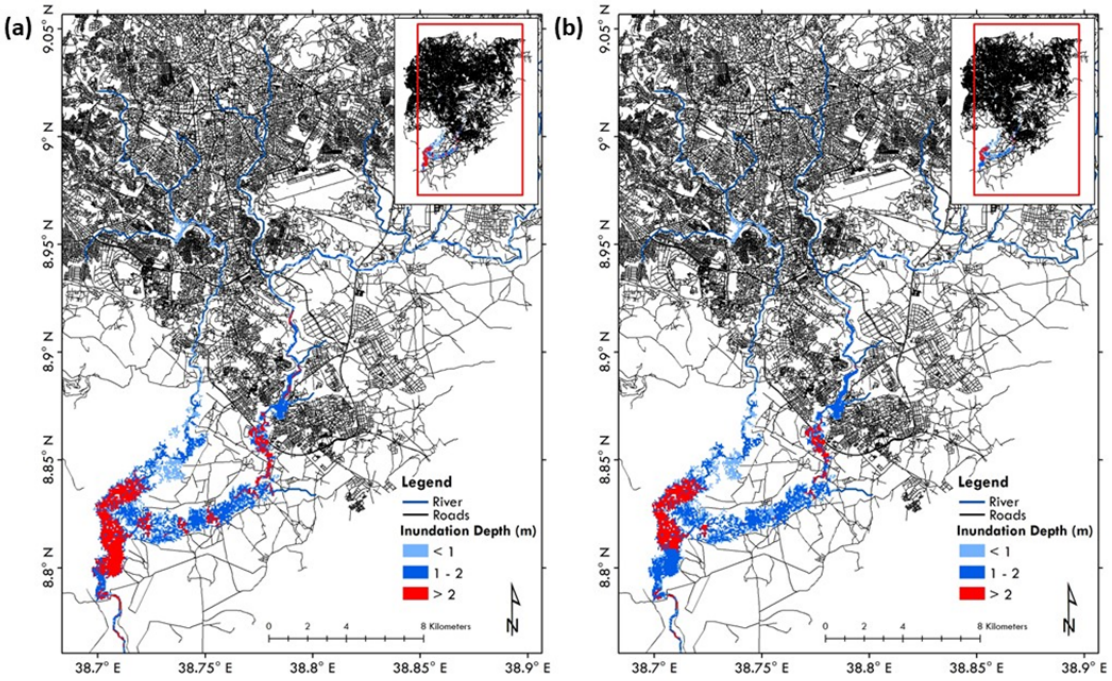

Figure 15. Flood inundation depth for Addis-Ababa city in Ethiopia under WACCM model and (b) Flood inundation depth for Addis-Ababa city in Ethiopia under ARISE-SAI model.

For Nairobi and Kampala, however, projections reveal minimal differences in flood depths between albedo-modified and non-albedo conditions, suggesting that the effectiveness of albedo interventions may vary depending on local climatic and urban characteristics.

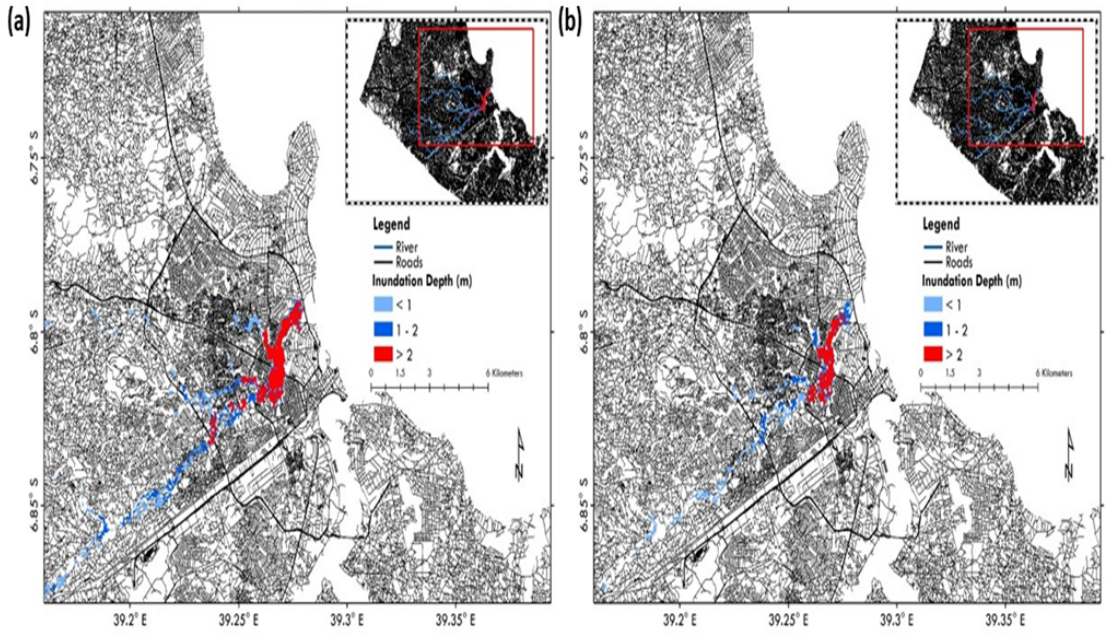

Figure 16. Flood inundation depths for Dar es Salaam City, Tanzania, under WACCM6 (a) and ARISE-SAI (b) models.

The implications of these findings are profound as deep and widespread flooding is associated with population displacement, damage to property, and severe disruption of urban systems and services. Vulnerable populations, particularly those residing in informal settlements, are dispropor-

 doi:10.20944/preprints202603.0667.v1

tionately exposed to these risks due to limited adaptive capacity and inadequate infrastructure. In Dar es Salaam, a city with a history of recurrent flood events [52], the results indicate that more than 37,000 people are likely to be affected by flood inundation depths exceeding 2m. In contrast, projected inundation depths of 0.5–1.0m are estimated to impact over 70,000 people in Kampala and more than 200,000 people in Nairobi (Figure 17).

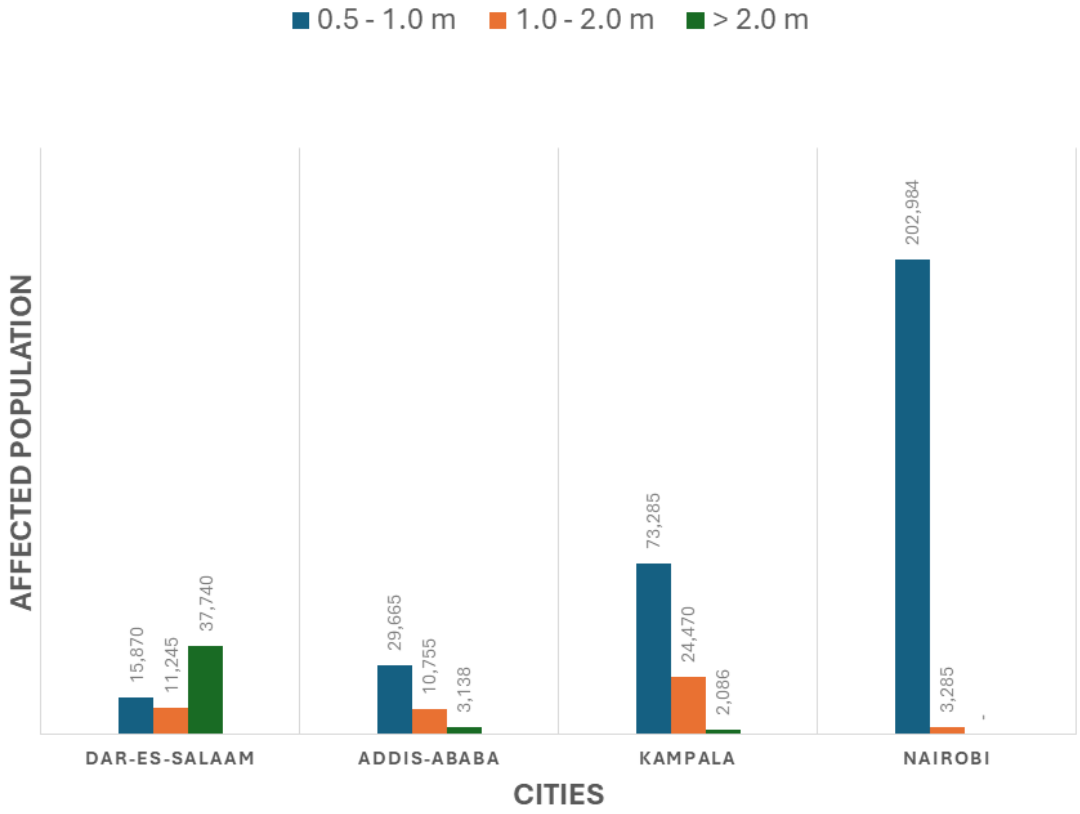

Figure 17. Projected population potentially affected by simulated flood events at varying inundation depths across the four major cities in Eastern Africa under a global warming scenario without albedo modification.

Furthermore, the assessment of projected flood impacts on road infrastructure indicates that residential road networks are consistently the most affected across all major cities in Eastern Africa (Figure 18), followed by secondary and tertiary road classes. Disruption to these critical transport corridors is likely to exacerbate flood impacts by impeding emergency response, humanitarian assistance, and post-disaster recovery efforts. Collectively, these projections underscore the urgent need to integrate climate-resilient urban planning, sustainable and flood-resilient infrastructure development, and robust disaster preparedness strategies into future urban growth and climate adaptation pathways.

 doi:10.20944/preprints202603.0667.v1

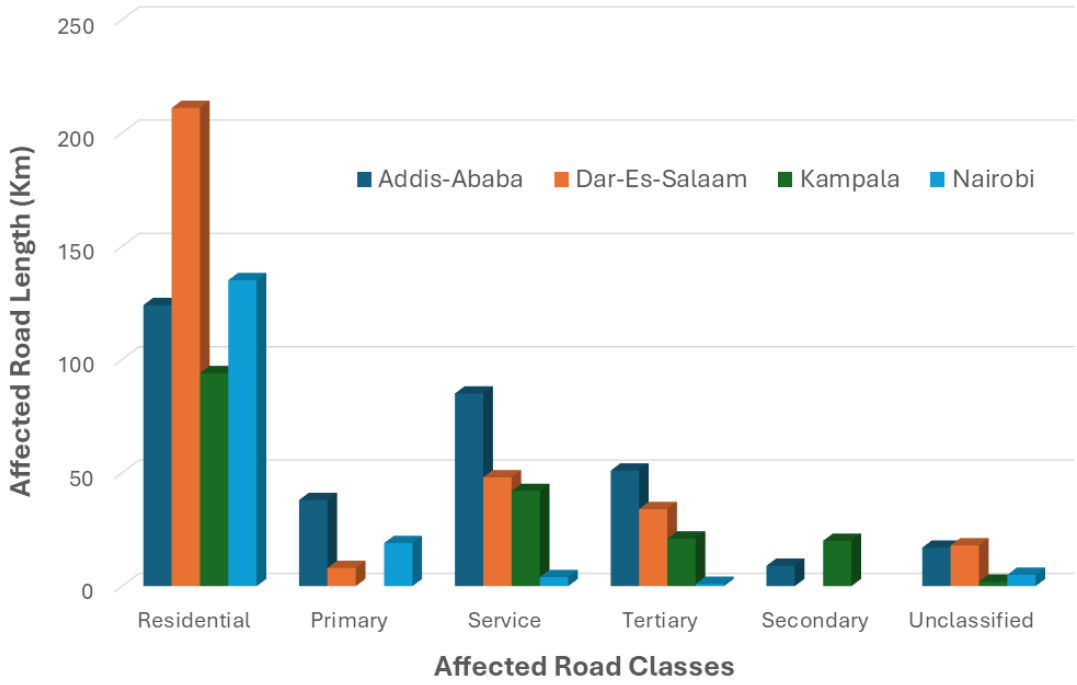

Figure 18. Projected roads potentially affected by simulated flood events at inundation depths greater than 1.5m across the four major cities in Eastern Africa under a global warming scenario without albedo modification.

4. Discussion

This study investigated the interannual variability of rainfall across the four largest cities in Eastern Africa and evaluated the performance of the Rainfall–Runoff–Inundation (RRI) model in simulating flood dynamics and identifying inundation hotspots. In addition, both historical and projected flood extents were analysed, and inundation depths were simulated to inform regional flood risk assessment. The results indicate that recent decades have experienced increasingly pronounced rainfall extremes, reflecting a growing intensification of hydrometeorological variability in the region. Although these recent extremes cannot be attributed solely to anthropogenic climate change, mounting evidence suggests that climate change is influencing both climate variability and the frequency and magnitude of extreme hydrometeorological events [53]. From an adaptation perspective, particular attention should be directed toward compound extremes, as the assessment of flood risks through a compound-event framework provides a more integrated understanding of cascading and multi-hazard phenomena [54].

Meteorological extremes that drive high-impact hazards, such as flash floods, often occur abruptly, providing limited lead time for early warnings, and are typically confined to small catchments spanning only a few hundred square kilometres. These events exhibit strong spatial heterogeneity and occur over short temporal scales [55,56]. However, General Circulation Models (GCMs) lack the spatial resolution required to adequately represent rainfall processes at local or catchment scales, as these processes are governed by fine-scale topographic, convective, and land–atmosphere interactions that demand high-quality observational data.

To bridge this scale gap, a statistical downscaling approach was employed in this study to translate coarse-resolution GCM rainfall outputs to a regional scale more representative of local hydrological processes. The comparison of downscaled results with raw GCM simulations revealed that statistical downscaling substantially reduced rainfall biases. Nevertheless, such statistical approaches are constrained by their inherent assumption of stationarity—that is, the persistence of historical relationships between large-scale climate predictors and local-scale rainfall responses. Under future non-stationary

 doi:10.20944/preprints202603.0667.v1

climate conditions, this assumption may weaken, potentially resulting in the underestimation of extreme rainfall events and associated hydrological impacts.

Emerging methodologies—such as physics-informed machine learning (ML) models and convection-permitting (CP) simulations at higher temporal and spatial resolutions—offer promising avenues for overcoming these limitations. These approaches can better capture localized convective processes and compound extreme events, thereby improving the physical realism of rainfall projections. However, their broader application remains constrained by significant computational requirements and the limited availability of consistent, high-quality observational datasets necessary for model training, calibration, and validation.

The accurate representation of hydrological processes in numerical models also depends critically on the availability and reliability of observed data for calibration and validation. In East Africa, however, data scarcity, inconsistency, and limited accessibility remain persistent challenges. In this study, for example, the lack of access to key observational datasets—particularly in Uganda—due to institutional data-sharing restrictions impeded comprehensive model calibration.

Furthermore, the choice of the hydrological modelling framework influences the applicability and temporal scope of the simulations. The RRI model, utilized in this study, is an event-based model that performs effectively in simulating individual flood events but is less suited for long-term, continuous hydrological assessments. Consequently, the analysis was confined to simulating extreme flood events over representative 30-year historical and future periods. Conducting continuous multi-decadal hydrological simulations would require substantial computational resources to process the large datasets involved.

4.1. Recommendations for future research

1. Adopt convection-permitting climate simulations for both SAI and non-SAI scenarios to better capture convective processes and reduce uncertainties associated with precipitation—recognized as the largest source of uncertainty in future flash flood projections [57];
2. Explore alternative hydrological modelling frameworks capable of ensemble-based flood forecasting, such as the Ensemble Framework for Flash Flood Forecasting (EF5). EF5 integrates multiple water balance models and routing schemes, enabling the generation of ensemble predictions of streamflow, unit streamflow (streamflow normalized by basin area), and soil saturation [58];

5. Conclusions

Early warning systems based on calibrated and validated hydrological models offer a critical pathway for reducing flood-related risks in urban environments. Reliable forecasts of river flow and inundation dynamics can enable timely preparedness and response actions among urban residents, particularly in flood-prone areas. The availability of comprehensive information on integrated watershed management, land-use change, climate impacts, and the expected frequency, extent, depth, and trajectory of floods is therefore essential for enhancing anticipatory action and adaptive capacity.

The overarching aim of this study was to quantify the extent to which meteorological and climatic drivers—particularly extreme rainfall—contribute to flood occurrence in the major cities of Eastern Africa, using Rainfall–Runoff–Inundation (RRI) model simulations under both baseline and Stratospheric Aerosol Injection (SAI) scenarios. The modelling results indicate that urban populations in the four major cities are likely to face heightened flood risks in the future, with disproportionate impacts expected among low-income communities residing in informal settlements. These impacts include recurrent displacement, loss of property, and disruption of livelihoods.

Beyond highlighting the exposure of vulnerable populations, the findings underscore the necessity of integrating infrastructure development, disaster preparedness, and climate-resilient urban planning into regional development frameworks. Moreover, the model simulations suggest that solar geoengineering through albedo modification may have potential in moderating the adverse impacts of flooding under future climate conditions in Eastern Africa's urban centres.

 doi:10.20944/preprints202603.0667.v1

Nevertheless, the understanding of SAI's broader impacts on regional climate and hydrological extremes remains constrained by several factors. These include:

1. Limitations in modelling capabilities — current models struggle to accurately represent convective rainfall processes, particularly within small catchments and at sub-daily time scales;
2. Knowledge and capacity gaps — there remains limited expertise among hydrologists in the region regarding the effective application of SAI and high-resolution climate datasets for impact studies, highlighting the need for strengthened collaboration between hydrologists and meteorologists; and;
3. 3. Data scarcity and accessibility constraints — insufficient availability and limited access to reliable observational and impact datasets hinder model calibration, validation, and comprehensive impact assessment.

Addressing these limitations through enhanced regional data-sharing mechanisms, capacity building, and the adoption of high-resolution convection-permitting modelling approaches will be vital for improving future flood risk assessments and for evaluating the broader hydrological implications of emerging climate intervention technologies such as SAI.

Author Contributions: Conceptualization, Franklin J. Opijah, Herbert O. Misiani, Betty N. Barasa, Hussen S. Endris and Jully O. Ouma.; methodology, Franklin J. Opijah, Herbert O. Misiani, Betty N. Barasa, Hussen S. Endris and Jully O. Ouma.; validation, Franklin J. Opijah, Herbert O. Misiani, Betty N. Barasa, Hussen S. Endris and Jully O. Ouma.; formal analysis, Herbert O. Misiani, Betty N. Barasa, Hussen S. Endris and Jully O. Ouma.; writing—original draft preparation, Betty N. Barasa, Jully O. Ouma and Herbert O. Misiani.; writing—review and editing, Franklin J. Opijah, Herbert O. Misiani, Betty N. Barasa, Hussen S. Endris, Jully O. Ouma and Christopher Lennard.; visualization, Herbert O. Misiani, Betty N. Barasa, Hussen S. Endris and Jully O. Ouma.; supervision, Franklin J. Opijah and Christopher Lennard.; project administration, Franklin J. Opijah.; funding acquisition, Franklin J. Opijah, Herbert O. Misiani, Betty N. Barasa, Hussen S. Endris and Jully O. Ouma. All authors have read and agreed to the published version of the manuscript.

Funding: This work was supported by the Degrees Modelling Fund (formerly the DECIMALS Fund) Grant under the World Academy of Sciences [Contract Number: 4500445436].

Data Availability Statement: ARISE-SAI data are available at https://doi.org/10.5065/9kcn-9y79 and SSP2-4.5 data are available at https://doi.org/10.26024/0cs0-ev98.

Acknowledgments: The climate material is based upon work supported by the National Science Foundation National Centre for Atmospheric Research (NSF NCAR), which is a major facility sponsored by the National Science Foundation under Cooperative Agreement no. 1852977 and by Silver Lining through its Safe Climate Research Initiative. The Community Earth System Model (CESM) project is supported primarily by the National Science Foundation. Computing and data storage resources, including the Cheyenne supercomputer (doi:10.5065/D6RX99HX), were provided by the Computational and Information Systems Laboratory (CISL) at NSF NCAR.

Conflicts of Interest: The authors declare no conflicts of interest. The funders had no role in the design of the study; in the collection, analyses, or interpretation of data; in the writing of the manuscript; or in the decision to publish the results.

References

1. Feller, U.; Vaseva, I.I. Extreme climatic events: impacts of drought and high temperature on physiological processes in agronomically important plants. *Frontiers in Environmental Science* **2014**, *2*, 39. https://doi.org/10.3389/fenvs.2014.00039.
2. Schreck III, C.J.; Semazzi, F.H. Variability of the recent climate of eastern Africa. *International Journal of Climatology: A Journal of the Royal Meteorological Society* **2004**, *24*, 681–701. https://doi.org/10.1002/joc.1019.
3. Hansen, G.; Stone, D. Assessing the observed impact of anthropogenic climate change. *Nature Climate Change* **2016**, *6*, 532–537. https://doi.org/10.1038/nclimate2896.

 doi:10.20944/preprints202603.0667.v1

4. Sun, Q.; Zhang, X.; Zwiers, F.; Westra, S.; Alexander, L.V. A global, continental, and regional analysis of changes in extreme precipitation. *Journal of Climate* **2021**, *34*, 243–258. https://doi.org/10.1175/JCLI-D-19-0892.1.
5. Meehl, G.A.; Zwiers, F.; Evans, J.; Knutson, T.; Mearns, L.; Whetton, P. Trends in extreme weather and climate events: issues related to modeling extremes in projections of future climate change. *Bulletin of the American Meteorological society* **2000**, *81*, 427–436. https://doi.org/10.1175/1520-0477(2000)081<0427:TIEWAC>2.3.CO;2.
6. Planton, S.; Déqué, M.; Chauvin, F.; Terray, L. Expected impacts of climate change on extreme climate events. *Comptes Rendus Geoscience* **2008**, *340*, 564–574. https://doi.org/10.1016/j.crte.2008.07.009.
7. Reed, C.; Anderson, W.; Kruczkiewicz, A.; Nakamura, J.; Gallo, D.; Seager, R.; McDermid, S.S. The impact of flooding on food security across Africa. *Proceedings of the National Academy of Sciences* **2022**, *119*, e2119399119. https://doi.org/10.1073/pnas.2119399119.
8. Kalantari, Z.; Ferreira, C.S.S.; Keesstra, S.; Destouni, G. Nature-based solutions for flood-drought risk mitigation in vulnerable urbanising parts of East-Africa. *Current Opinion in Environmental Science & Health* **2018**, *5*, 73–78. https://doi.org/10.1016/j.coesh.2018.06.003.
9. Du, S.; Shi, P.; Van Rompaey, A.; Wen, J. Quantifying the impact of impervious surface location on flood peak discharge in urban areas. *Natural Hazards* **2015**, *76*, 1457–1471. https://doi.org/10.1007/s11069-014-1463-2.
10. Kelly, D.A. Impact of paved front gardens on current and future urban flooding. *Journal of flood risk management* **2018**, *11*, S434–S443. https://doi.org/10.1111/jfr3.12231.
11. Ayugi, B.; Dike, V.; Ngoma, H.; Babaousmail, H.; Mumo, R.; Ongoma, V. Future changes in precipitation extremes over East Africa based on CMIP6 models. *Water* **2021**, *13*, 2358. https://doi.org/10.3390/w13172358.
12. Shongwe, M.E.; van Oldenborgh, G.J.; et al. Projected changes in mean and extreme precipitation in Africa under global warming. Part II: Southern Africa. *Journal of Climate* **2011**, *24*, 3718–3733. https://doi.org/10.1175/2010JCLI2883.1.
13. Ezeh, A.; Kissling, F.; Singer, P. Why sub-Saharan Africa might exceed its projected population size by 2100. *The Lancet* **2020**, *396*, 1131–1133. https://doi.org/10.1016/S0140-6736(20)31522-1.
14. Taye, M.T.; Dyer, E. Hydrologic extremes in a changing climate: A review of extremes in East Africa. *Current Climate Change Reports* **2024**, *10*, 1–11. https://doi.org/10.1007/s40461-024-00193-9.
15. Hagos, Y.G.; Andualem, T.G.; Yibeltal, M.; Mengie, M.A. Flood hazard assessment and mapping using GIS integrated with multi-criteria decision analysis in upper Awash River basin, Ethiopia. *Applied Water Science* **2022**, *12*, 148. https://doi.org/10.1007/s13201-022-01674-8.
16. Gebrechorkos, S.H.; Peng, J.; Dyer, E.; et al. Global high-resolution drought indices for 1981–2022. *Earth System Science Data* **2023**, *15*, 5449–5466. https://doi.org/10.5194/essd-15-5449-2023.
17. Jevrejeva, S.; Jackson, L.P.; Grinsted, A.; Lincke, D.; Marzeion, B. Flood damage costs under the sea level rise with warming of 1.5 C and 2 C. *Environmental Research Letters* **2018**, *13*, 074014. https://doi.org/10.1088/1748-9326/aacc76.
18. Paltan, H.; Allen, M.; Haustein, K.; Fuldauer, L.; Dadson, S. Global implications of 1.5 C and 2 C warmer worlds on extreme river flows. *Environmental Research Letters* **2018**, *13*, 094003. https://doi.org/10.1088/1748-9326/aad985.
19. Irvine, P.J.; Kravitz, B.; Lawrence, M.G.; Muri, H. An overview of the Earth system science of solar geoengineering. *Wiley Interdisciplinary Reviews: Climate Change* **2016**, *7*, 815–833. https://doi.org/10.1002/wcc.423.
20. Hulme, M. Climate change: Climate engineering through stratospheric aerosol injection. *Progress in Physical Geography* **2012**, *36*, 694–705. https://doi.org/10.1177/0309133312456414.
21. Irvine, P.J.; Ridgwell, A.; Lunt, D.J. Climatic effects of surface albedo geoengineering. *Journal of Geophysical Research: Atmospheres* **2011**, *116*, D24112. https://doi.org/10.1029/2011JD016281.
22. Kuebbeler, M.; Lohmann, U.; Feichter, J. Effects of stratospheric sulfate aerosol geo-engineering on cirrus clouds. *Geophysical Research Letters* **2012**, *39*, L23803. https://doi.org/10.1029/2012GL053797.
23. Latham, J.; Bower, K.; Choularton, T.; et al. Marine cloud brightening. *Philosophical Transactions of the Royal Society A* **2012**, *370*, 4217–4262. https://doi.org/10.1098/rsta.2012.0086.
24. McInnes, C.R. Space-based geoengineering: challenges and requirements. *Proceedings of the Institution of Mechanical Engineers, Part C: Journal of Mechanical Engineering Science* **2010**, *224*, 571–580. https://doi.org/10.1243/09544062JMES1439.

 doi:10.20944/preprints202603.0667.v1

25. Storelvmo, T.; Kristjánsson, J.E.; Muri, H.; et al. Cirrus cloud seeding has potential to cool climate. *Science* **2014**, *339*, 1219–1222. https://doi.org/10.1126/science.1226368.
26. Alamou, E.A.; Zandagba, J.E.; Biao, E.I.; Obada, E.; Da-Allada, C.Y.; Bonou, F.K.; Pomalegni, Y.; Baloitcha, E.; Tilmes, S.; Irvine, P.J. Impact of stratospheric aerosol geoengineering on extreme precipitation and temperature indices in West Africa using GLENS simulations. *Journal of Geophysical Research: Atmospheres* **2022**, *127*. https://doi.org/10.1029/2021JD035855.
27. Misiani, H.O.; Endris, H.S.; Opijah, F.J.; et al. Simulated response of the climate of eastern Africa to stratospheric aerosol intervention. *Frontiers in Climate* **2025**, *7*, 1522235. https://doi.org/10.3389/fclim.2025.1522235.
28. Patel, T. Potential impact of stratospheric aerosol geoengineering on projected temperature and precipitation extremes in South Africa. Master's thesis, University of Cape Town, Cape Town, South Africa, 2021. Accessed: 2025-10-17.
29. Pinto, I.; Jack, C.; Lennard, C.; Tilmes, S.; Odoulami, R.C. Africa's climate response to solar radiation management with stratospheric aerosol. *Geophysical Research Letters* **2020**, *47*, e2019GL086047. https://doi.org/10.1029/2019GL086047.
30. Wei, L.; Ji, D.; Miao, C.; Muri, H.; Moore, J.C. Global streamflow and flood response to stratospheric aerosol geoengineering. *Atmospheric Chemistry and Physics* **2018**, *18*, 16033–16050. https://doi.org/10.5194/acp-18-16033-2018.
31. Tilmes, S.; Fasullo, J.; Lamarque, J.F.; Marsh, D.R.; Mills, M.; Alterskjaer, K.; Muri, H.; Kristjánsson, J.E.; Boucher, O.; Schulz, M.; et al. The hydrological impact of geoengineering in the Geoengineering Model Intercomparison Project (GeoMIP). *Journal of Geophysical Research: Atmospheres* **2013**, *118*, 11–036. https://doi.org/10.1002/jgrd.50868.
32. Cheng, L.; Zhu, J.; Abraham, J.; Trenberth, K.E.; Fasullo, J.; Zhang, B.; Yu, F.; Wan, L.; Chen, X.; Song, X. 2018 Continues Record Global Ocean Warming. *Advances in Atmospheric Sciences* **2019**, *36*, 249–252. https://doi.org/10.1007/s00376-019-8276-x.
33. Niemeier, U.; Schmidt, H.; Timmreck, C. The dependency of geoengineered sulfate aerosol on the emission strategy. *Atmospheric Chemistry and Physics* **2013**, *13*, 911–923. https://doi.org/10.1002/asl.304.
34. Ngome, C.S.; Yeom, C. Impacts of Floods on Sustainable Urban Development in Kenya: The Case of Nairobi and Mombasa. *Asia-Pacific Journal of Convergence Research* **2024**, *10*, 147–160.
35. Trento Oliveira, L.; Kuffer, M.; Belgiu, M.; Dijkstra, A.M. Diagnostics of urban flooding in Nairobi, 2024. https://doi.org/10.5281/zenodo.14650088.
36. Funk, C.; Peterson, P.; Landsfeld, M.; et al. The climate hazards infrared precipitation with stations: a new environmental record for monitoring extremes. *Scientific Data* **2015**, *2*, 1–21. https://doi.org/10.1038/sdata.2015.66.
37. Themeßl, M.J.; Gobiet, A.; Heinrich, G. Empirical-statistical downscaling and error correction of regional climate models. *Climatic Change* **2012**, *112*, 449–468. https://doi.org/10.1007/s10584-011-0224-4.
38. Bourgault, P.; Huard, D.; Smith, T.J.; Logan, T.; Aoun, A.; Lavoie, J.; Dupuis, E.; Rondeau-Genesse, G.; Alegre, R.; Barnes, C.; et al. xclim: xarray-based climate data analytics. *Journal of Open Source Software* **2023**, *8*, 5415. https://doi.org/10.21105/joss.05415.
39. Cannon, A.J.; Sobie, S.R.; Murdock, T.Q. Bias Correction of GCM Precipitation by Quantile Mapping: How Well Do Methods Preserve Changes in Quantiles and Extremes. *Journal of Climate* **2015**, *28*, 6938–6959. https://doi.org/10.1175/JCLI-D-14-00754.1.
40. Sayama, T. Rainfall-Runoff-Inundation Analysis for Flood Risk Assessment at the Regional Scale. In Proceedings of the Proc. of the 5th Conference of Asian Pacific Hydrology and Water Resources (APHW), 2010, pp. 568–576. https://doi.org/10.2208/jscej1949.1962.79_15.
41. Sayama, T.; Ozawa, G.; Kawakami, T.; Nabesaka, S.; Fukami, K. Rainfall–runoff–inundation analysis of the 2010 Pakistan flood in the Kabul River basin. *Hydrological Sciences Journal* **2012**, *57*, 298–312. https://doi.org/10.1080/02626667.2011.644245.
42. Ishihara, T.; Takasao, T. A Study on the Sub-Surface Runoff and its Effects on Runoff Process. *Transactions of the Japan Society of Civil Engineers* **1962**, *1962*, 15–23. https://doi.org/10.2208/jscej1949.1962.79_15.
43. Takasao, T.; Shiiba, M. Incorporation of the effect of concentration of flow into the kinematic wave equations and its applications to runoff system lumping. *Journal of Hydrology* **1988**, *102*, 301–322. https://doi.org/10.1016/0022-1694(88)90104-7.

 doi:10.20944/preprints202603.0667.v1

44. Nastiti, K.D.; Kim, Y.; Jung, K.; An, H. The Application of Rainfall-Runoff-inundation (RRI) Model for Inundation Case in Upper Citarum Watershed. *Procedia Engineering* **2015**, *125*, 166–172. https://doi.org/10.1016/j.proeng.2015.11.024.
45. Herath, R.D.; Pawar, U.; Aththanayake, D.M.; et al. Rainfall-runoff-inundation (RRI) model for Kalu River, Sri Lanka. *Modeling Earth Systems and Environment* **2024**, *10*, 1825–1839. https://doi.org/10.1007/s40808-023-01877-1.
46. Sayama, T.; Tatebe, Y.; Tanaka, S. An emergency response-type rainfall-runoff-inundation simulation for 2011 Thailand floods. *Journal of Flood Risk Management* **2017**, *10*, 65–78. https://doi.org/10.1111/jfr3.12147.
47. Willmott, C.J. On the Evaluation of Model Performance in Physical Geography. In *Spatial Statistics and Models*; Springer, 1984; Vol. 40. https://doi.org/10.1007/978-94-017-3048-8_23.
48. Krause, P.; Boyle, D.P.; Bäse, F. Comparison of different efficiency criteria for hydrological model assessment. *Advances in Geosciences* **2005**, *5*, 89–97. https://doi.org/10.5194/adgeo-5-89-2005.
49. Diro, G.T.; Grimes, D.I.F.; Black, E. Large Scale Features Affecting Ethiopian Rainfall. In *Climate Change and Food Security in Ethiopia*; Springer, 2011; pp. 13–50. https://doi.org/10.1007/978-90-481-3842-5_2.
50. Kilavi, M.; MacLeod, D.; Ambani, M.; et al. Extreme rainfall and flooding over central Kenya including Nairobi city during the long-rains season 2018: causes, predictability, and potential for early warning and actions. *Atmosphere* **2018**, *9*, 472. https://doi.org/10.3390/atmos9120472.
51. Mwangi, J.; Okello, L.; Tadesse, G. Simulation and Assessment of Flood Risk in Major Cities of Eastern Africa Using the RRI Model and Bias-Corrected Rainfall Data. *International Journal of Hydrology and Climate Science* **2024**, *12*, 145–168.
52. Sakijege, T.; Dakyaga, F. Going beyond generalisation: perspective on the persistence of urban floods in Dar es Salaam. *Natural Hazards* **2023**, *115*, 1909–1926. https://doi.org/10.1007/s11069-022-05645-9.
53. Thornton, P.K.; Ericksen, P.J.; Herrero, M.; Challinor, A.J. Climate variability and vulnerability to climate change: a review. *Global Change Biology* **2014**, *20*, 3313–3328. https://doi.org/10.1111/gcb.12581.
54. Zscheischler, J.; Westra, S.; Van Den Hurk, B.J.; et al. Future climate risk from compound events. *Nature Climate Change* **2018**, *8*, 469–477. https://doi.org/10.1038/s41558-018-0156-3.
55. Sene, K. Flash Floods. In *Hydrometeorology*; Springer, Cham, 2016. https://doi.org/10.1007/978-3-319-23546-2_9.
56. Kelsch, M. Hydro-meteorological characteristics of flash floods. In *Coping with Flash Floods*; Kluwer Academic Publishers, 2001; pp. 181–193. https://doi.org/10.1007/978-94-010-0918-8_18.
57. Hapuarachchi, H.A.P.; Wang, Q.J.; Pagano, T.C. A review of advances in flash flood forecasting. *Hydrological Processes* **2011**, *25*, 2771–2784. https://doi.org/10.1002/hyp.8040.
58. Flamig, Z.L.; Vergara, H.; Gourley, J.J. The ensemble framework for flash flood forecasting (EF5) v1. 2: Description and case study. *Geoscientific Model Development* **2020**, *13*, 4943–4958. https://doi.org/10.5194/gmd-13-4943-2020.